JOURNAL OF SYNCHROTRON RADIATION

ISSN 1600-5775

Establishment of new design criteria for GlidCop® X-ray absorbers

Jeff T. Collins,* Jeremy Nudell, Gary Navrotski, Zunping Liu and Patric Den Hartog

Advanced Photon Source, Argonne National Laboratory, 9700 South Cass Avenue, Argonne, IL 60439, USA.
*Correspondence e-mail: collins@aps.anl.gov

Received 22 August 2016
Accepted 1 February 2017

Edited by S. Svensson, Uppsala University, Sweden

Keywords: GlidCop®; thermal fatigue life; photon absorbers; high heat load; front-ends; design criteria; transient non-linear FEA.

An engineering research program has been conducted at the Advanced Photon Source (APS) in order to determine the thermomechanical conditions that lead to crack formation in GlidCop®, a material commonly used to fabricate X-ray absorbers at X-ray synchrotron facilities. This dispersion-strengthened copper alloy is a proprietary material and detailed technical data of interest to the synchrotron community is limited. The results from the research program have allowed new design criteria to be established for GlidCop® X-ray absorbers based upon the thermomechanically induced fatigue behavior of the material. X-ray power from APS insertion devices was used to expose 30 GlidCop® samples to 10000 thermal loading cycles each under various beam power conditions, and all of the samples were metallurgically examined for crack presence/geometry. In addition, an independent testing facility was hired to measure temperature-dependent mechanical data and uniaxial mechanical fatigue data for numerous GlidCop® samples. Data from these studies support finite element analysis (FEA) simulation and parametric models, allowing the development of a thermal fatigue model and the establishment of new design criteria so that the thermomechanically induced fatigue life of X-ray absorbers may be predicted. It is also demonstrated how the thermal fatigue model can be used as a tool to geometrically optimize X-ray absorber designs.

1. Introduction

Hard X-ray synchrotron facilities commonly use GlidCop® to fabricate X-ray absorbers such as photon shutters, masks and slit assemblies. GlidCop® is an attractive material for the fabrication of X-ray absorbers because it has 93% of the thermal conductivity of pure copper, the yield strength and ultimate tensile strengths are equivalent to those of mild-carbon steel, the material is cyclically stable, even at elevated temperatures, and it does not undergo a significant amount of hardening or softening even after thousands of thermal cycles (Troxell, 1989; Mitchell, 1996). GlidCop® AL-15 (UNS-C15715) used in this study is a proprietary aluminium oxide dispersion-strengthened copper alloy, and thermomechanical data and fatigue data of interest to the synchrotron community available in the open literature are limited.

The existing Advanced Photon Source (APS) design criteria for GlidCop® X-ray absorbers limit the maximum temperature to 300°C, allow only single-phase cooling water (no boiling), and limit the maximum von Mises stress to 400 MPa for photon shutters. The maximum von Mises stress allowed for fixed masks under extreme missteering conditions is relatively relaxed since such missteering cases are very rare. The water pressure at the APS after going through two-thirds of the length of a typical photon shutter is about 0.414 MPa (60 psig), and the corresponding water boiling temperature at

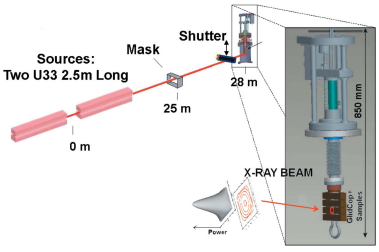

this pressure is 153°C. Constant room-temperature material properties are used in the linear steady-state finite element analysis (FEA). Although these design criteria for GlidCop® X-ray absorbers have been successful in avoiding component failures over the 20 year life of the facility, the APS and other facilities contemplate upgrades that may result in higher thermal loads on the X-ray absorbers. Consequently, efforts have been made to establish less conservative, more realistic design criteria based on the thermomechanically induced fatigue limits of GlidCop®. A number of studies have been conducted over the past several years in the synchrotron community to try to develop new design criteria for GlidCop® X-ray absorbers (Ravindranath *et al.*, 2006; Takahashi *et al.*, 2008). The study presented here complements previous studies and sufficient data are now available to allow new design criteria to be established for GlidCop® X-ray absorbers based upon the thermomechanically induced fatigue behavior of the material.

As Manson pointed out in 1966, thermal fatigue is quite different from mechanical fatigue for a number of reasons, one being the presence of inadvertent stress concentration factors in thermal fatigue tests that are absent in mechanical fatigue tests. Thermal fatigue tests will yield fewer cycles to failure than mechanical fatigue tests, even when the upper bound temperature of the thermal fatigue tests does not exceed the temperature at which the mechanical fatigue tests were conducted (Manson, 1966). To illustrate, a plastic strain range *versus* number of cycles to failure log–log plot of Manson's original data is shown in Fig. 1. The dashed line represents the thermal fatigue tests where the samples were cycled between 200°C and 500°C (350°C mean temperature), and the solid lines represent mechanical fatigue tests conducted at various temperatures. It is evident that the number of cycles to failure for the thermal fatigue tests are significantly less than those achieved with the mechanical fatigue tests, even for one mechanically cycled at 600°C. However, the slopes of all of the data sets are nearly identical and can be made coincident through experimentally determined scaling factors. Therefore, a mechanical fatigue model can be used as a starting point to develop a thermal fatigue model based on observed damage from thermal fatigue tests performed under actual operating conditions.

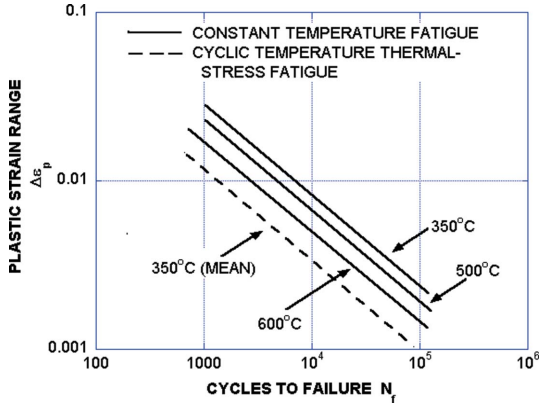

Figure 1
Plastic strain range *versus* number of cycles to failure for mechanical and thermal fatigue tests; from Manson (1966).

For this study, several tasks were performed in parallel and used as the basis for the development of a thermal fatigue model for GlidCop® AL-15. Temperature-dependent uniaxial mechanical fatigue data were obtained for GlidCop® AL-15, and these data were used to develop a mechanical fatigue model. Temperature-dependent true stress *versus* true strain data were also obtained for GlidCop® AL-15 in both tension and compression, and the data were used in all transient non-linear FEA performed for this study. Using X-ray power from the APS, numerous GlidCop® AL-15 test samples were subjected to severe cyclic thermal loading under various beam power conditions, and these test samples were metallurgically examined for crack presence/geometry. A temperature-dependent mechanical fatigue model was developed and used as the base to develop a thermal fatigue model by matching observed damage on the thermal fatigue test samples with life cycle predictions based on mean temperature. This process allowed 'failure' to be defined and quantified based on thermal fatigue model predictions and observed damage to the samples.

Transient non-linear FEA was performed on each test sample in order to determine the total strain range and peak temperature data required for the thermal fatigue model. Similar analysis was performed on all of the existing APS front-end photon shutter designs in order to assess life cycle predictions under various operating conditions. Based upon this analysis, new design criteria for GlidCop® AL-15 have been established, and it is demonstrated how the thermal fatigue model can be used as a tool to geometrically optimize X-ray absorber designs.

2. Mechanical testing of GlidCop® AL-15

Westmoreland Mechanical Testing and Research, Inc. (http://www.wmtr.com), an independent testing company, was contracted to conduct all of the GlidCop® AL-15 mechanical testing. Temperature-dependent uniaxial mechanical fatigue data were obtained for GlidCop® AL-15 in accordance with ASTM E606-12. Temperature-dependent true stress *versus* true strain data were obtained for GlidCop® AL-15, in both tension and compression, in accordance with ASTM E21-09 and ASTM E209-89a (2000), respectively. All tests were conducted in a pure argon gas environment. The samples were all machined from 12.7 mm × 162 mm GlidCop® AL-15 LOX[1] extruded flat plate, the same material used in many of the APS photon shutter designs for beam strike surfaces.

2.1. True stress *versus* true strain testing

True stress *versus* true strain tests were conducted on GlidCop® AL-15 samples in both tension and compression at seven different temperatures including room temperature and

[1] Low Oxygen GlidCop® contains an additional 250 p.p.m. boron and is recommended for braze joints or extended high-temperature vacuum applications.

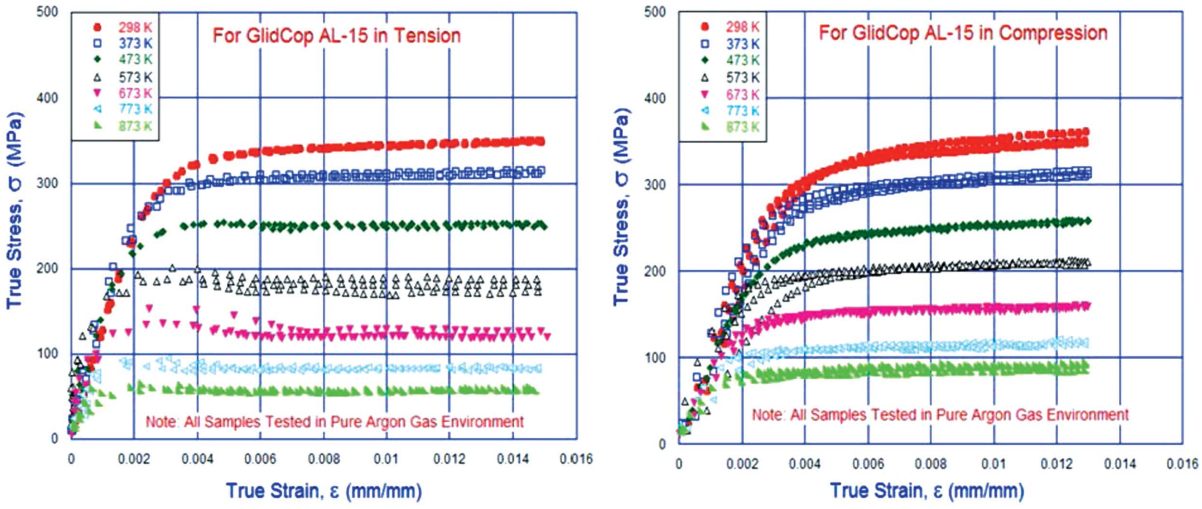

Figure 2
Temperature-dependent true stress *versus* true strain data for GlidCop® AL-15 in tension and compression.

373 K to 873 K in 100 K increments. Three different samples were tested at each temperature condition, both in tension and compression. Fig. 2 shows the temperature-dependent true stress *versus* true strain results for tests done in both tension and compression. Up to a test temperature of approximately 573 K the true stress *versus* true strain results are similar, and at higher temperatures less stress is required to produce the same strain for GlidCop® AL-15 in tension compared with in compression. It should be noted here that the true stress at elevated temperature is always less than at room temperature, and the previous practice of elastically evaluating the maximum von Mises stress using room-temperature material properties generates meaningless and possibly misleading results. Curve fits for these data sets have been generated and were used in all transient non-linear FEA performed for this research program.

2.2. Uniaxial mechanical fatigue testing and analysis

Uniaxial mechanical fatigue tests were conducted on GlidCop® AL-15 samples at four different test temperatures. Numerous total strain range test points were chosen at each test temperature to ensure that the data would span the range of interest from several hundred cycles to failure up to 20000 cycles to failure. A total of 45 samples were tested. Linear regression and a method of least squares were used to process the data on the basis of relating the total strain range to the sum of the plastic and elastic strain ranges. The elastic strain range is approximated by Basquin's law (Basquin, 1910) and the plastic strain range is approximated by the Manson–Coffin equation (Manson, 1966). The uniaxial mechanical fatigue model, relating the total strain range to the sum of the elastic and plastic strain ranges, is shown in equation (1),

$$\frac{\Delta\varepsilon_t}{2} = \frac{\Delta\varepsilon_{elastic} + \Delta\varepsilon_{plastic}}{2} = \frac{\sigma_f'}{E}(2N_f)^b + \varepsilon_f'(2N_f)^c, \quad (1)$$

where $\Delta\varepsilon_t/2$ is the total strain range, σ_f' is the fatigue strength coefficient, E is the elastic modulus (Young's modulus), N_f is the number of cycles to failure, b is the fatigue strength exponent, ε_f' is the fatigue ductility coefficient and c is the fatigue ductility exponent. The coefficient for Basquin's law is the ratio of the fatigue strength coefficient divided by the elastic modulus (σ_f'/E). Temperature-dependent data for the elastic modulus were obtained from the mechanical fatigue tests conducted by Westmoreland Mechanical Testing and Research, Inc. The fatigue strength coefficient (σ_f') is found by using the temperature-dependent y-intercept values from the fatigue strength exponent data reduction. The exponent for Basquin's law, referred to as the fatigue strength exponent (b), is derived by plotting the log of the elastic strain amplitude *versus* the log of the number of stress/strain reversals, and then finding a common slope for the four temperature-dependent data sets such that the overall R^2 value, a measure of goodness-of-fit of linear regression, is maximized.

Similarly, the coefficient for the Manson–Coffin equation, referred to as the fatigue ductility coefficient (ε_f'), is found by using the temperature-dependent y-intercept values from the fatigue ductility exponent data reduction. The exponent for the Manson–Coffin equation, referred to as the fatigue ductility exponent (c), is derived by plotting the log of the plastic strain amplitude *versus* the log of the number of stress/strain reversals and maximizing the R^2 value.

A plot of the total strain range ($\Delta\varepsilon_t$) *versus* the number of cycles to failure (N_f) from the uniaxial mechanical fatigue tests on GlidCop® AL-15 is shown in Fig. 3. The mechanical fatigue model is shown at the bottom of the plot where the temperature variable (T) in the equation is the isothermal test temperature in Kelvin. The solid lines in the plot are the predictions using the mechanical fatigue model for each isothermal test temperature, and it can be seen that good agreement exists between the data and the predictions. The fatigue strength/elastic modulus coefficient (σ_f'/E) for the elastic strain range equation was found to be ($0.67 - T/2000$), and the value for the fatigue strength exponent (b) was found to be -0.066. The fatigue ductility coefficient (ε_f') for the

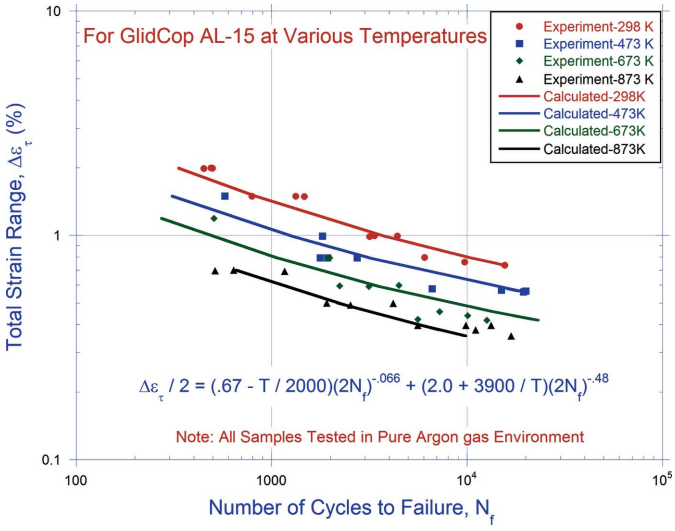

Figure 3
Temperature-dependent uniaxial mechanical fatigue data for GlidCop® AL-15.

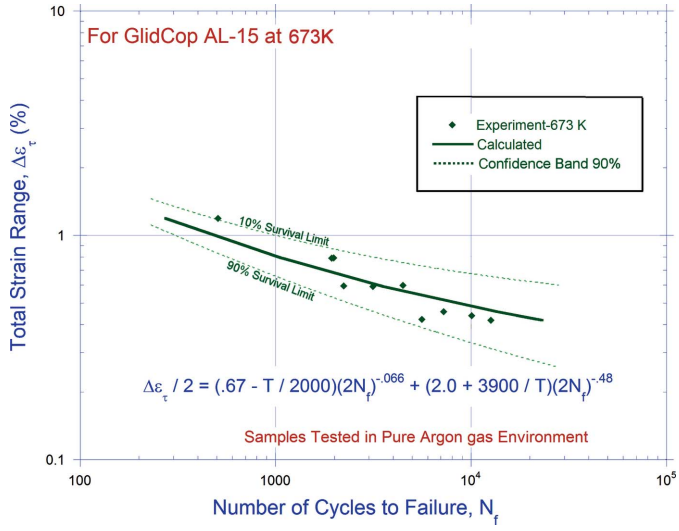

Figure 4
90% confidence band for fatigue of GlidCop® AL-15 at 673 K.

plastic strain range equation was found to be $(2.0 + 3900/T)$, and the value for the fatigue ductility exponent (c) was found to be -0.48. The mechanical fatigue model for GlidCop® AL-15 was used as a base to develop a thermal fatigue model.

Takahashi *et al.* (2008) found that the fatigue ductility exponent, c (referred to as α in their study), for the Manson–Coffin equation is dependent upon environmental test conditions. Tests conducted in air yielded a different value for the fatigue ductility exponent than tests conducted in a vacuum. Unlike samples tested in air, samples tested in a vacuum are not exposed to oxygen that can cause oxidation at elevated temperatures, leading to initiation sites where surface cracks can develop. In this study, a value of -0.48 was independently determined for the fatigue ductility exponent, identical to the value reported by Takahashi *et al.* This demonstrates that tests performed in a pure argon gas environment yield similar results as tests conducted in a vacuum.

Due to the highly statistical nature of the fatigue process, it was important to analyze and integrate the limitations imposed by a finite data set into the development of a fatigue criterion. Confidence bands for each of the data sets at a 90% prediction interval were calculated for the family of curves using the standard assumption of a log-normal probability distribution as illustrated in Fig. 4. The width of this prediction band systematically varies as a function of temperature. To good approximation, the width of the band decreases by 33% for the 473 K data fit and decreases another 33% for the 298 K fit. Conversely, the band increases by 33% for the 873 K data. A more technically exact analysis using Weibull statistics was possible for 298 K and 873 K data when analysed separately but was not possible for the multi-temperature data as a family. These Weibull confidence bands are 50% narrower than those shown with the 10% survival limit much closer to the mean. This gives assurance that the confidence band shown in Fig. 4 is a conservative calculation by more than a factor of 2.

2.3. Cyclic strain hardening

Another useful piece of information that can be obtained from the uniaxial mechanical fatigue test data is the establishment of the cyclic strain hardening relation for GlidCop® AL-15. The cyclic strain hardening relation is given in equation (2),

$$\sigma = K\Delta\varepsilon_{\rm p}{}^{n}, \tag{2}$$

where σ is the applied stress, K is the cyclic strain hardening coefficient, $\Delta\varepsilon_{\rm p}$ is the resulting plastic strain and n is the cyclic strain hardening exponent (Hollomon, 1945). The cyclic strain hardening exponent is a measure of how a material hardens from applied strain. A cyclic strain hardening exponent equal to zero means the material is a perfect plastic solid, whereas a cyclic strain hardening exponent equal to 1 means the material is a perfect elastic solid. The plot on the left in Fig. 5 shows the cyclic strain hardening coefficient (K) *versus* temperature, and the plot on the right shows the log of the applied stress *versus* the log of the resulting plastic strain used to determine the cyclic strain hardening exponent (n). The cyclic strain hardening exponent was found to be 0.10 and the cyclic strain hardening coefficient was found to be $730 - 0.64T$, where T is the isothermal test temperature in Kelvin. In comparison, annealed high-conductivity copper typically has a cyclic strain hardening exponent equal to 0.44, whereas the value is 0.15 for annealed 4340 steel (Low & Garofalo, 1947). This illustrates how GlidCop® AL-15 behaves very differently than copper even though it is made up mostly of copper.

2.4. Modification of the uniaxial fatigue equation for thermal fatigue applications

The temperature-dependent uniaxial mechanical fatigue model for GlidCop® AL-15 shown in Fig. 3 is transformed into a thermal fatigue model by redefining the temperature variable in the equation as suggested by Taira (1973). Whereas the isothermal test temperature is used in the mechanical

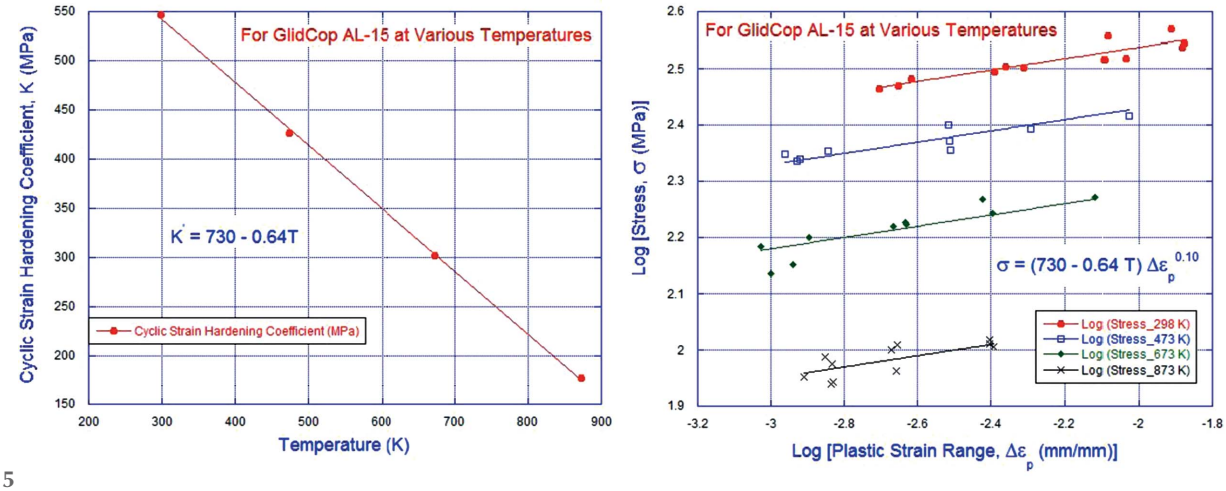

Figure 5
Cyclic strain hardening relation for GlidCop® AL-15.

fatigue model, the mean temperature between the maximum surface temperature and the cooling water temperature is used in the thermal fatigue model. Equation (3) provides the final form of the thermal fatigue model for GlidCop® AL-15,

$$\frac{\Delta\varepsilon_t}{2} = \left(0.67 - \frac{T_m}{2000}\right)(2N_f)^{-0.066} + \left(2.0 + \frac{3900}{T_m}\right)(2N_f)^{-0.48}, \quad (3)$$

where $\Delta\varepsilon_t/2$ is the total strain amplitude in percent, N_f is the number of cycles to failure, and T_m is the mean temperature between the maximum surface temperature and the cooling water temperature in Kelvin.

3. Thermomechanically induced fatigue testing of GlidCop® AL-15

3.1. Experimental set-up and test sample configuration

A total of 30 GlidCop® AL-15 samples were subjected to 10000 thermal cycles, each at normal incidence, using X-ray beam delivered from two in-line 2.5 m-long APS 33.0 mm-period undulator-A devices. Various beam power loading conditions were applied to the samples to simulate a variety of operating conditions. Each test sample assembly consisted of four GlidCop® AL-15 blocks brazed to a common copper cooling tube loop, providing a total of eight test sites for each test sample assembly. Each sample block measured 101.6 mm (L) × 27.5 mm (H) × 22.2 mm (W), and the beam strike surfaces were finished to $R_a \simeq 0.4$ µm. Four test sites were provided on one side of the test sample assembly and, once rotated 180° inside of the UHV testing chamber, four more test sites were made available for testing on the other side of the test piece assembly. The X-ray beam passed through an upstream fixed mask with an aperture size of 4.5 mm × 4.5 mm located 25.124 m from the source point. At the power levels important to this study, this mask allows the full two-dimensional Gaussian cone of the central X-ray beam to pass while clipping low power-density tails beyond $\sim 4\sigma$. The UHV test chamber was located 28.122 m from the source point, and an upstream voice coil-activated photon shutter was used to control the beam exposure cycle time. The experimental set-up is shown in Fig. 6.

Prior to the experiments, transient non-linear FEA was performed on a typical test sample in order to determine the required thermal cycle heating and cooling times. In all of the transient non-linear FEA analyses performed for this study, the measured true stress *versus* true strain data were used in the analysis along with temperature-dependent properties for thermal conductivity, specific heat, thermal expansion coefficient and Young's modulus. The transient non-linear FEA showed that a 1.4 s heating time and 9 s cooling time are sufficient to achieve near steady-state total strain range. It was also determined that the peak compressive stress is achieved in less than 0.1 s during the heating cycle. Compared with previous studies (Ravindranath *et al.*, 2006), the shorter heating and cooling times allowed us to test many more GlidCop® AL-15 samples in the beam time allotted to conduct this study. Consequently, a large statistical database is available to determine the thermomechanically induced

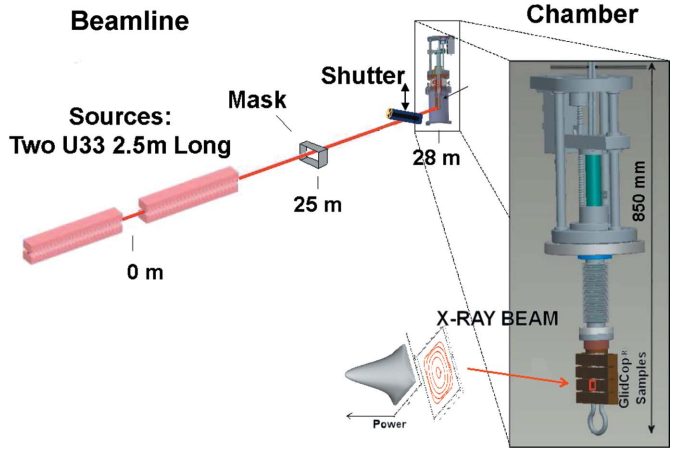

Figure 6
Experimental set-up used for thermomechanically induced fatigue testing at the APS.

fatigue behavior of GlidCop® AL-15 under a wide range of beam power loading conditions.

3.2. Experimental results

After the tests were completed, surface images were obtained for all the GlidCop® AL-15 test samples and, in order to assess crack geometry, metallurgical sectioning was performed on all samples. Transient non-linear FEA was performed for each thermal load condition in order to determine the total strain range and peak surface temperature for each test sample. The mean temperature and the total strain range were then used in the thermal fatigue model to predict the estimated number of cycles to failure for each test sample. A typical equivalent stress *versus* total strain range hysteresis loop obtained from the non-linear FEA using *ANSYS*, employing the multi-linear kinematic hardening model, is provided in Fig. 7. If the yield point is exceeded, the strain caused by the first heating cycle plastically deforms the material causing kinematic strain hardening to occur, and this locally increases the yield strength of the material. As can be seen in the figure, only a few thermal cycles are required for the total strain range to converge to a constant value, and therefore only four load cycles were required for each simulation.

It was discovered after testing a number of samples that the beam was not symmetrically centred in the exit mask but instead was offset by 0.53 mm (H) × 1.18 mm (V). The beam was realigned for all subsequent sample tests. Calorimetry was performed for both the offset beam cases and the aligned beam cases, and the beam location on each sample was accounted for during the transient non-linear FEA. The calorimetry data, plotted as normalized total absorbed power *versus* undulator gap setting, for the aligned and offset beam cases along with the theoretical available beam power are provided in Fig. 8.

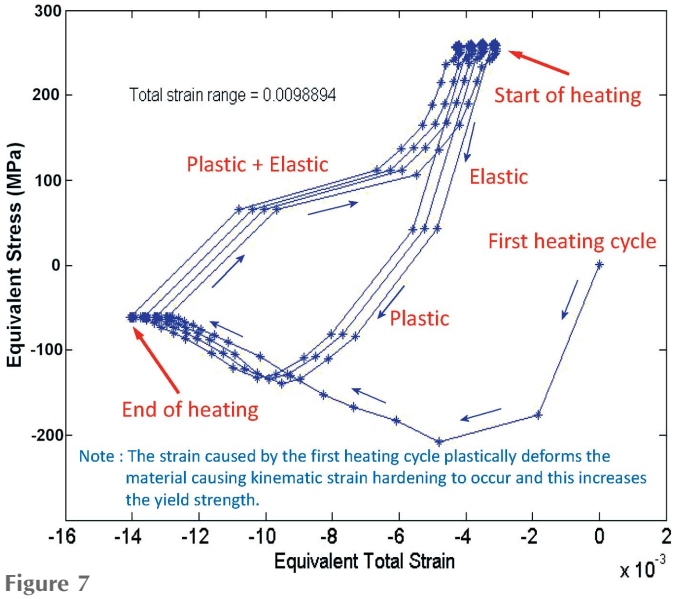

Figure 7
Typical equivalent stress *versus* total strain range hysteresis loop for a GlidCop® AL-15 test sample.

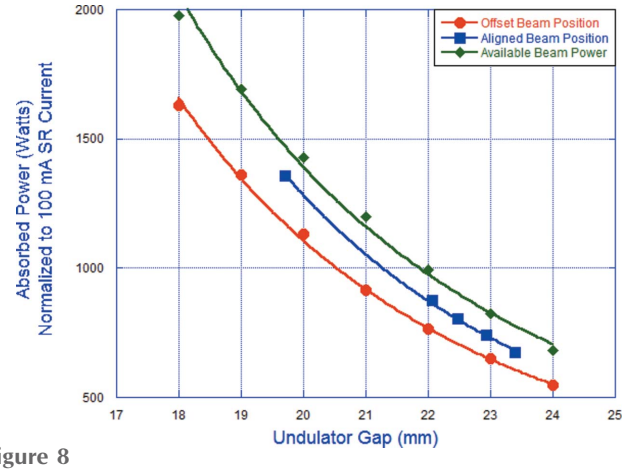

Figure 8
Calorimetry data for the aligned and offset beam cases compared with the available beam power.

The test sample database for this study is provided in Fig. 9, arranged in order of increasing thermal load. Samples highlighted in green are for the cases where the beam was properly aligned, whereas samples highlighted in pink are for the cases where the beam was offset. Where applicable, information obtained from metallurgical sectioning is provided for measurements of the largest crack length, width and depth for each sample. Observations on the sample surface conditions after testing are provided in the comments section. The total strain range and peak surface temperature for each sample obtained through transient non-linear FEA along with the estimated number of cycles to failure obtained from the thermal fatigue model are also provided.

The red arrow on the right-hand side of Fig. 9 indicates where the thermal fatigue model for GlidCop® AL-15 predicts 10000 cycles to failure, and sample groups 1, 2, 3 and 4, indicated on the left-hand side of Fig. 9, surround this point. Samples in group 1 have no detectable surface degradation, whereas some of the samples in groups 2, 3 and 4 have 'cat scratches' with the possibility of small shallow cracks that are less than 2 mm in surface length. Cat scratches are shallow regions of surface grain drop-out that are the result of surface thermal compression ejecting weakly bound copper grain remnants (grain remnants are 4 to 7 µm thick; partial grain fragments remain after machining operations to create the beam strike surface). GlidCop® AL-15 is extruded in the manufacturing process and consequently the copper grains are long and thin, with dimensions on the order of several micrometers in diameter and millimeters in length. The copper grains are always aligned in the direction of the extrusion. The cat scratches observed through the metallurgical surface imaging performed on sample 1 are shown in Fig. 10. Multiple parallel linear cat scratches can be observed on several of the GlidCop® AL-15 test samples, and at higher thermal loads or longer cycles one of the cat scratches will become dominant and provide a site for crack initiation.

The experimentally observed damage to the test samples in groups 2, 3 and 4 coupled with predictions from the thermal fatigue model of equation (3) allow 'failure' after 10000

	Sample Number	Total Absorbed Power (W)	Peak Heat Flux (W/mm^2)	Total Strain Range (%)	Maximum Temperature , 1.4s heating (K)	Mean Temperature (K)	Largest Crack Length (μm)	Largest Crack Width (μm)	Largest Crack Depth (μm)	Comments	Estimated Number of Cycles to Failure
	37	690	101	0.407	685	492				No surface degredation	179,000
	38	690	101	0.407	685	492				No surface degredation	179,000
	34	754	109	0.468	719	509				No surface degradation	48,100
	35	754	109	0.468	719	509				No surface degradation, 5 superficial <200 μm cat scratches	48,100
1	20	758	123	0.530	749	524				No surface degradation	18,100
1	21	758	123	0.530	749	524				No surface degradation	18,100
1	22	758	123	0.530	749	524				No surface degradation	18,100
1	23	758	123	0.530	749	524				No surface degradation	18,100
1	24	758	123	0.530	749	524				No surface degradation, 10 superficial <200 μm cat scratches	18,100
2	32	816	116	0.534	752	525				8 small "cat scratches"	17,300
2	33	816	116	0.534	752	525	892	47	95	Several "cat scratches", 1 small shallow crack	17,300
3	1	818	130	0.604	782	540	1815	11	106	7 "cat scratches", 5 small shallow cracks	7,650
3	9	818	130	0.604	782	540	1238	32	236	3 small shallow cracks	7,650
3	10	818	130	0.604	782	540	453	11	49	"Cat scratches" and small shallow cracks	7,650
3	11	818	130	0.604	782	540				Many "cat scratches", no cracks	7,650
3	14	878	137	0.678	815	557	916	41	No x-section	Several "cat scratches" and possible cracks	3,880
4	29	881	123	0.609	785	542				13 "cat scratches", no cracks	7,220
4	30	881	123	0.609	785	542	747	43	37	5 "cat scratches", 1 small shallow crack	7,220
4	31	881	123	0.609	785	542				>20 "cat scratches", no cracks	7,220
	6	924	142	0.735	840	569	2989	56	631	13 "cat scratches", 1 long deep crack, 2 small shallow cracks	2,510
	7	1032	154	0.869	897	598	2531	56	No x-section	Many "cat scratches", several long deep cracks	1,110
	4	1142	166	0.989	956	627	4329	53	1622	>15 "cat scratches",1 long deep crack	609
	16	1142	166	0.989	956	627	3227	224	1218	Many "cat scratches", 1 long deep crack, 4 small shallow cracks	609
	44	1272	160	1.049	980	639	2554	117	447	Surface "bulging", 2 long deep cracks, 1 small shallow crack	475
	45	1386	171	1.146	1034	666	1708	108	456	Surface "rumpling", several long deep cracks	320
	46	1386	171	1.146	1034	666	4792	34	2121	Numerous long deep cracks and melting	320
	43	1509	181				3623			Numerous long deep cracks and melting	
	41	1784	204				4624			Numerous long deep cracks and melting	
	42	2092	228				5269			Numerous long deep cracks and melting	
	47	4680	428				9668			Numerous long deep cracks and melting	

Beam offset .53mm H x 1.18mm V
Beam centered

Figure 9
Test sample data base for thermomechanically induced fatigue in GlidCop® AL-15 studies.

thermal cycles to be defined and quantified. For X-ray absorbers made from GlidCop® AL-15, 'failure' is defined as the presence of cat scratches with the possibility of small shallow cracks not exceeding 2 mm in surface length. This definition of 'failure' is consistent with the criteria adopted at SPring-8 based upon Japanese industrial standards (Takahashi *et al.*, 2008; JIS, 1992).

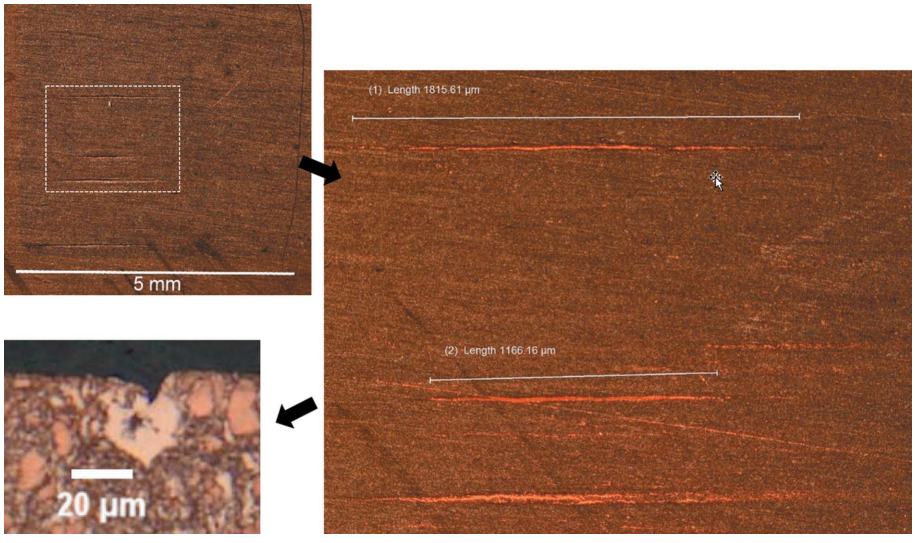

Figure 10
Typical superficial 'cat scratch' pattern on a GlidCop® AL-15 test sample (#1) caused by surface grain remnant drop-out. The top left-hand photograph illustrates the visual appearance under normal lighting conditions and the origin of the designation cat scratch. The right-hand image shows a magnified bright-field view. The bottom left-hand image shows a highly magnified cross section through the upper 1.8 mm-long scratch.

4. Transient non-linear FEA for APS front-end photon shutters

In addition to the analysis performed on all of GlidCop® AL-15 test sample cases, transient non-linear FEA was also performed on all of the front-end photon shutter designs in operation at the APS. Both the existing maximum design conditions and, where applicable, the maximum multi-bend achromat (MBA) lattice baseline conditions currently planned for the APS Upgrade (APS-U) were considered. Similar to the process used to determine sufficient heating and cooling times for the GlidCop® AL-15 test samples, transient non-linear FEA was performed on a typical photon shutter and it was determined that a 10 s heating time and 40 s cooling time are sufficient

to achieve near steady-state total strain range. It was also determined that the peak compressive stress is achieved in less than a few seconds during the heating cycle. Time is not a variable in the thermal fatigue model, and therefore for each transient non-linear FEA performed on the photon shutters a steady-state thermal simulation was performed first. This provided the maximum surface temperature required to calculate the mean temperature that is needed for the thermal fatigue model [equation (3)]. The results from the transient non-linear FEA performed on the APS photon shutters are provided in Fig. 11. All of these photon shutters intercept the X-ray beam at shallow grazing incidence angles (column 3) on flat GlidCop® AL-15 beam strike surfaces. Each photon shutter has a series of water-cooling channels underneath the beam strike surface characterized by the minimum cooling wall thickness (column 4). The first- and second-generation APS photon shutters are represented by P2-20 and P2-30, respectively, and modern photon shutter designs used at the APS are represented by the high-heat-load (HHL) shutter and the canted undulator shutter.

The existing APS uses primarily 33.0 mm-period undulators, and so the cases where these types of undulators are referenced in the source parameters (column 2) consider the existing maximum design conditions for the different photon shutter designs (Trakhtenberg *et al.*, 2004; Jaski, 2005). The worst-case source for thermal loading being considered for the APS-U are shorter-period 27.5 mm undulators. The cases in the source parameters column where these undulators are referenced consider conditions well beyond the proposed maximum MBA lattice baseline conditions of 200 mA ring current. The mean temperature, determined through steady-state thermal analysis, and the total strain range, determined through transient non-linear FEA, are used in the thermal fatigue model to estimate the number of cycles to failure, provided in the far right column in Fig. 11.

The thermal fatigue model predicts over 20000 cycles to 'failure' for all of the APS photon shutter cases considered in Fig. 11. The water boils (wall temperature >153°C) at 137 mA operation for the P2-20 photon shutter and thus it can only be operated slightly beyond maximum design conditions of 130 mA storage ring current with a single 33 mm-period undulator. The P2-30 photon shutter, the HHL photon shutter and the canted undulator photon shutter can all be operated well beyond the MBA lattice baseline conditions of 200 mA ring current with dual in-line 27.5 mm-period undulators. Except for the case of the canted undulator photon shutter operating at existing maximum design conditions (200 mA ring current with dual canted 33 mm-period undulators and 1 mrad beam separation), all of the photon shutter cases considered experience plastic deformation as evident by the fact that the peak tensile stress (column 10) is not zero. In this case, the canted undulator photon shutter operating at existing maximum design conditions never enters plasticity evident by the fact that the peak tensile stress is zero. This is a case where the strain caused by the first heating cycle was insufficient to plastically deform the material, and therefore the yield stress of the material remained unchanged.

The canted undulator shutter operating at 330 mA, well beyond maximum proposed MBA lattice baseline conditions (dual canted 27.5 mm-period undulators and 1 mrad beam

Photon Shutter Type	Source Parameters	Grazing Incidence Angle (degrees)	Minimum Cooling Wall Thickness (mm)	Total Absorbed Power (W)	Peak Heat Flux (W/mm^2)	Maximum Temperature (°C)	Maximum Cooling Wall Temperature (°C)	Mean Temperature (K)	Peak Compressive / Tensile Stress (MPa)	Elastic Strain Range (%)	Plastic Strain Range (%)	Total Strain Range (%)	Estimated Number of Cycles to Failure
P2-20	Single U33.0 130 mA	2.00	6.35	6,780	18	315	147	443	-205 / 236	0.358	0.0688	0.427	152,000
P2-20	Single U33.0 137 mA	2.00	6.35	7,130	19	331	154	451	-211 / 250	0.366	0.0917	0.458	101,000
P2-30	Single U33.0 225 mA	1.68	10.60	11,900	33	290	95	431	-211 / 247	0.366	0.0958	0.462	114,000
P2-30	Dual In-Line U27.5 275 mA	1.68	10.60	25,100	36	393	121	482	-204 / 252	0.373	0.104	0.477	53,500
HHL Shutter	Dual In-Line U33.0 180 mA	1.05	9.00	14,600	25	248	92	410	-205 / 173	0.309	0.00615	0.315	9.57E+06
HHL Shutter	Dual In-Line U27.5 392 mA	1.05	9.00	25,500	32	375	133	473	-215 / 287	0.381	0.173	0.554	20,800
Canted Undulator Shutter	Dual Canted U33.0 with 1 mrad Beam Separation 200 mA	1.05	9.00	19,900	10	248	130	410	-202 / 0	0.265	0	0.265	1.03E+08
Canted Undulator Shutter	Dual Canted U27.5 with 1 mrad Beam Separation 330 mA	1.05	9.00	20,400	16	332	154	451	-185 / 97	0.234	0	0.234	3.28E+08

Figure 11
Results from transient non-linear FEA performed on APS photon shutters.

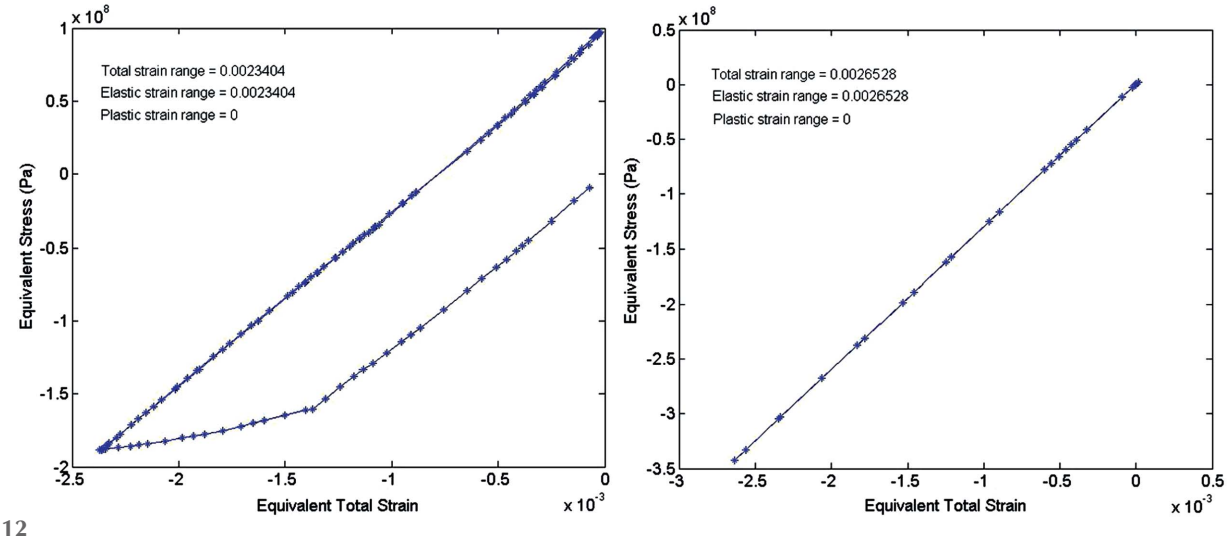

Figure 12
Equivalent stress *versus* total strain range hysteresis loop plots for the canted undulator photon shutter cases: maximum MBA lattice baseline conditions (left) and maximum existing design conditions (right).

separation), offers an interesting case where the material was plastically deformed on the first heating cycle, but this caused kinematic strain hardening to occur in the material, locally increasing the yield stress. Therefore, for subsequent thermal cycles the yield stress was increased enough on the first beam strike such that the resulting strain was purely elastic thereafter. Note here that the resulting plastic strain range (column 12) is zero and that the total strain range (column 13) is purely elastic. The equivalent stress *versus* total strain range hysteresis loops for the two canted undulator photon shutter cases are shown in Fig. 12.

5. Using the thermal fatigue model as a tool to geometrically optimize X-ray absorber designs

Parameters such as cooling wall thickness, grazing incidence angle, cooling channel layout *etc*. can be optimized through parametric transient non-linear FEA studies using the thermal fatigue model [equation (3)]. Therefore, the thermal fatigue model can be used to geometrically optimize component designs in order to reduce cost, weight and component length. To demonstrate the optimizing process, the HHL photon shutter was considered and the grazing incidence angle was incrementally varied from the current design angle of 1.05° up to a grazing incidence angle of 2.08° in several increments as shown in Fig. 13. It is evident that the reduction in life cycle (column 11) drops dramatically with increase in grazing incidence angle (column 1). At the same time the reduction in shutter length (column 2) with increase in grazing incidence angle reaches a point of diminishing returns relative to the dramatic reduction in life cycle. It can be concluded that the optimum grazing incidence angle for the HHL photon shutter is somewhere around 2.0°. Increasing the grazing incidence angle beyond this will not significantly decrease the photon shutter length; however, the estimated number of cycles to 'failure' will rapidly diminish. Coupled with transient non-linear FEA, the thermal fatigue model offers a powerful tool for geometrically optimizing component designs.

6. The establishment of new design criteria for GlidCop® AL-15 X-ray absorbers

New design criteria have been established for GlidCop® AL-15 X-ray absorbers based upon the results of this study and the transient non-linear FEA performed on all of the APS front-end photon shutters. Whereas the previous design criteria for GlidCop® AL-15 X-ray absorbers limited the maximum temperature and the maximum von Mises stress, the new design criteria do not impose a maximum design temperature or stress but instead limit the minimum number of cycles to 'failure' as predicted by the thermal fatigue model for GlidCop® AL-15 [equation (3)]. Temperature and stress

Grazing Incidence Angle (degrees)	Shutter Length (mm)	Peak Heat Flux (W/mm^2)	Maximum Temperature (°C)	Maximum Cooling Wall Temperature (°C)	Mean Temperature (K)	Peak Compressive / Tensile Stress (MPa)	Elastic Strain Range (%)	Plastic Strain Range (%)	Total Strain Range (%)	Estimated Number of Cycles to Failure
1.05	648	17	199	80	385	-197 / 118	0.257	0	0.257	2.38E+08
1.5	556	24	277	103	424	-199 / 194	0.331	0.0185	0.350	390,000
1.75	526	28	320	116	446	-199 / 236	0.360	0.0735	0.434	37,900
2.08	496	33	377	132	474	-197 / 278	0.392	0.150	0.541	23,900

Figure 13
Optimizing the grazing incidence angle for the HHL shutter.

are included in the thermal fatigue model *via* the mean temperature and the total strain range. Although the new design criteria presented here are tailored for front-end photon absorbers, the foundation of the design criteria is the thermal fatigue model and it can be applied universally to aid in the design of any GlidCop® AL-15 X-ray absorber.

Similar to the previous design criteria, only single-phase cooling water is recommended. It is possible to design beyond the boiling point of the water if critical heat flux analysis is performed to ensure that a dry-out condition can never be reached under the worst-case operating conditions. However, at the present, the APS has no plans to pursue this option. From this analysis, it can be reasoned that a given component design could be further geometrically optimized by increasing the cooling wall thickness if boiling of the cooling water is the limiting design criteria.

X-ray absorbers can be designed to operate with a maximum surface temperature up to 405°C if transient non-linear FEA is performed to ensure that the number of cycles to 'failure' exceeds 20000 cycles using the thermal fatigue model. A temperature of 405°C, half the absolute temperature of the GlidCop® AL-15 melting point, is chosen as the maximum since it is the traditional limit where material creep considerations must be included (Manson & Halford, 2009). Therefore, the effects of creep do not need to be considered in the transient non-linear FEA if the maximum surface temperature does not exceed 405°C. However, transient non-linear FEA must be performed using true stress *versus* true strain data for GlidCop® AL-15 along with all relevant temperature-dependent material properties. A minimum of 20000 life cycles is the chosen threshold because no surface degradation is typically observed in this study when the estimated number of cycles to 'failure' is 20000 or more, as can be seen in Fig. 9. Some of the shutters in the APS have been in operation for years and may have already experienced several thousand applied thermal cycles.

In addition to the cases presented in Fig. 11, dozens of other cases have been evaluated at the APS where transient non-linear FEA has been applied to various absorber designs. This includes cases where very small focused beams (tens of micrometers spot size) with very high peak heat flux (>5 kW mm^{-2}), such as those generated at the Dynamic Compression Sector (https://dcs-aps.wsu.edu), are applied on an absorber at normal incidence. We have noted with all of these cases that if the maximum design temperature is limited to 375°C or less then the thermal fatigue model will always yield 20000 cycles or more to 'failure'. This should not be considered a universal rule, but can be used as a guideline while designing X-ray absorbers. Simple steady-state analysis can be performed to evaluate the maximum surface and cooling wall temperatures for a given X-ray absorber design, and the thermal fatigue model can be used as a final check to ensure that the proper minimum number of cycles to 'failure' are achieved.

To properly apply the new design criteria, beam strike surfaces shall be fabricated with a surface roughness of $R_a \leq 0.4$ µm, the surface condition used for both tensile and thermal fatigue testing. Fatigue damage initiation is generally known to be highly dependent on surface finish. However, this surface roughness specification can typically be achieved with a double mill pass on the beam strike surface during machining and will not add significantly to the fabrication costs. The new design criteria are intended for flat beam strike surfaces and, consequently, component designs that incorporate stress-concentrating features, such as small radius corners common in fixed mask designs, may achieve a fewer number of cycles to 'failure'.

7. Discussion

As an indication of the safety level build into the new design criterion, a 2014 survey of 25% of APS primary photon shutters experienced an average of 282 with a maximum of ~400 thermal cycles of any significance per year. Of those, only an average of 1.2% and maximum of 7.5% occurred at the full closed-gap power levels assumed during engineering design. Therefore, a minimum 20000 cycles to 'failure' threshold or equivalently a 50 year life assuming every thermal cycle occurs at maximum power is used as a conservative basis. As a benefit, the APS is considering the possibility of re-using some of the existing photon shutters for the APS-U.

There is a significant amount of safety built into the new design criteria established for GlidCop® AL-15 X-ray absorbers. The life-cycle predictions obtained from the thermal fatigue model assume that each beam strike occurs under worst-case operating conditions in exactly the same location on the beam strike surface. In reality, as pointed out by Takahashi *et al.* (2008), damage to the beam strike surface is cumulative, and each load cycle will consume a percentage of the life cycle. Few beamlines continuously operate under closed-gap conditions, and therefore many of the applied load cycles to a particular X-ray absorber may be far less severe than the worst-case load condition. Consequently, the number of cycles to 'failure' predicted by the thermal fatigue model is very conservative.

In addition, sample number 47 received 10000 thermal cycles under the worst-case possible conditions achievable at the APS using two in-line 33 mm-period undulators operating at 100 mA maximum storage ring current with closed gaps at 11.0 mm. The total beam power applied was 5258 W with 4680 W absorbed, more than 5.7 times the total beam power absorbed by the GlidCop® AL-15 test samples in the cat-scratch region (groups 2 and 3 in Fig. 9). As shown in Fig. 14, although the damage is significant, with evidence of surface extrusion, severe radial cracking, melting and evaporation, the maximum crack length was less than 10 mm and the maximum crack depth was less than 2 mm.

Modern GlidCop® AL-15 X-ray absorbers used at the APS, such as the HHL photon shutter and the canted undulator photon shutter, are designed with a 9 mm cooling wall thickness. The oldest X-ray photon shutter design in operation at the APS, the P2-20, has a cooling wall thickness of 6.35 mm. Considering that the worst-case crack depth obtained with

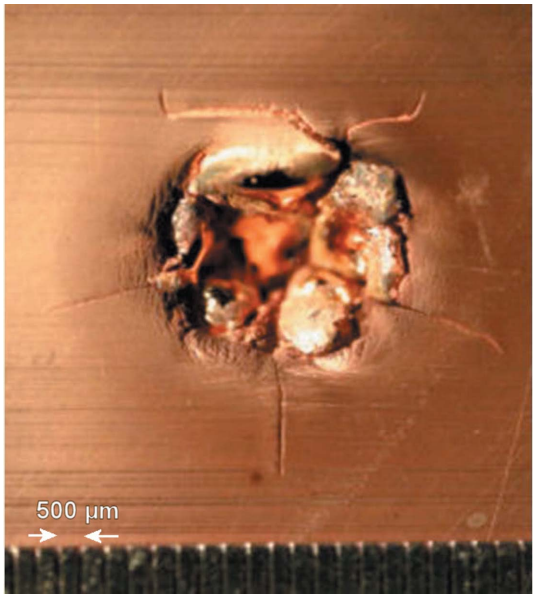

Figure 14
Sample 47 after 10000 thermal cycles under worst-case possible conditions.

sample 47 (Fig. 14) was less than 2 mm, and that this operating condition was many times greater than that of the 'failure' point established by the new design criteria for GlidCop® AL-15 X-ray absorbers, it is hard to imagine an operating scenario where a crack could ever propagate and reach a cooling channel wall if the new design criteria are followed. The new design criteria established for GlidCop® AL-15 X-ray absorbers are robust, and if employed will yield component designs that can withstand over 20000 cycles to 'failure', even if the beam power loading is applied under worst-case conditions. Generally, no surface degradation should be present at the end of the design life, or at worst a few cat scratches may be present on the beam strike surface with the possibility of small shallow cracks of less than 2 mm in surface length with crack depths of less than a few hundred micrometers.

8. Summary

Mechanical data were obtained for GlidCop® AL-15, quantifying the temperature-dependent true stress *versus* true strain and the low-cycle mechanical fatigue behavior of the material. The true stress *versus* true strain data obtained for GlidCop® AL-15 were used along with all other relevant temperature-dependent material properties to perform transient non-linear FEA on all of the test samples. A temperature-dependent mechanical fatigue model was derived for GlidCop® AL-15 and was used as a base to develop a thermal fatigue model by properly redefining the temperature variable in the model. Numerous GlidCop® AL-15 samples were subjected to 10000 thermal loading cycles under various beam conditions, and after metallurgical examination the predictions from the thermal fatigue model for each sample were matched with the observed damage in order to define and quantify 'failure'. Transient non-linear FEA was performed on all of the GlidCop® AL-15 test samples as well as all of the existing X-ray photon shutters in operation at the APS. Based upon the results of this study coupled with the transient non-linear FEA performed on all of the existing APS photon shutters in operation at the APS, new design criteria have been established for GlidCop® AL-15 X-ray absorbers. Furthermore, it was demonstrated how the thermal fatigue model can be used as a powerful tool to geometrically optimize component designs. There is a significant amount of safety built into the establishment of the new design criteria for GlidCop® AL-15 X-ray absorbers.

Acknowledgements

The authors would like to thank Mike Bosek, Kevin Knoerzer, Russ Otto, Bran Brajuskovic and Ali Khounsary for their technical efforts in the successful completion of this project. The authors would also like to thank Eric Jones from Westmoreland Mechanical Testing and Research, Inc. for his collaboration on this project. This work was supported by the US Department of Energy, Office of Science, under Contract No. DE-AC02-D6CH11357.

References

Basquin, O. H. (1910). *Proc. Am. Soc. Test. Mater.* **10**, 625–630.
Hollomon, J. H. (1945). *Trans. Am. Inst. Mech. Eng.* **162**, 268–277.
Jaski, Y. (2005). *Thermal Analysis of the Components of the Insertion Device Front Ends FEv1.2 and FEv.15.* Report ANL/APS/TB-50. Advanced Photon Source, Argonne National Laboratory, Argonne, Il, USA.
JIS (1992). *Method of High-Temperature Low-Cycle Testing for Metallic Materials.* Japanese Industrial Standard Z2279.
Low, J. R. & Garofalo, F. (1947). *Proc. Soc. Exp. Stress Anal.* **4**, 16–25.
Manson, S. S. (1966). *Thermal Stress and Low-Cycle Fatigue*, pp. 131–144; pp. 255–257. New York: McGraw-Hill.
Manson, S. S. & Halford, G. R. (2009). *Fatigue and Durability*, pp. 1–2. Materials Park: ASM International.
Mitchell, M. R. (1996). *ASM Handbook*, Vol. 19, *Fatigue and Fracture*, pp. 227–249. Materials Park: ASM International.
Ravindranath, V., Sharma, S., Rusthoven, B., Gosz, M., Zhang, L. & Biasci, J. (2006). *Proceedings of the International Workshop on Mechanical Engineering Design of Synchrotron Radiation Equipment and Instrumentation 2006 (MEDSI2006)*, 24–26 May 2006, Himeji, Hyogo, Japan.
Taira, S. (1973). *Fatigue at Elevated Temperatures, ASTM Special Technical Publication 520*, pp. 80–101. Philadelphia: American Society for Testing and Materials.
Takahashi, S., Sano, M., Mochizuki, T., Watanabe, A. & Kitamura, H. (2008). *J. Synchrotron Rad.* **15**, 144–150.
Trakhtenberg, E., Benson, C., Den Hartog, P. & Jaski, Y. (2004). *Third International Workshop on Mechanical Engineering Design of Synchrotron Radiation Equipment and Instrumentation (MEDSI2004)*, 24–27 May 2004, Grenoble, France. MEDSI-Proc-04-63.
Troxell, J. D. (1989). *Proceedings of the IEEE Thirteenth Symposium on Fusion Engineering*, 2–6 October 1989, Knoxville, TN, USA, pp. 761–765.